fibers

MDPI

Article

Effect of Polymer Concentration, Rotational Speed, and Solvent Mixture on Fiber Formation Using Forcespinning®

Nancy Obregon [1], Victor Agubra [2], Madhab Pokhrel [2], Howard Campos [2], David Flores [2], David De la Garza [2], Yuanbing Mao [1], Javier Macossay [1,*] and Mataz Alcoutlabi [2,*]

[1] Chemistry Department, The University of Texas Rio Grande Valley, Edinburg, TX 78539, USA; nancy.obregon01@utrgv.edu (N.O.); yuanbing.mao@utrgv.edu (Y.M.)

[2] Mechanical Engineering Department, The University of Texas Rio Grande Valley, Edinburg, TX 78539, USA; victor.agubra@utrgv.edu (V.A.); pokhrelmadhab@gmail.com (M.P.); howard.campos01@utrgv.edu (H.C.); david.e.flores01@utrgv.edu (D.F.); david.delagarza02@utrgv.edu (D.D.G.)

* Correspondence: javier.macossaytorres@utrgv.edu (J.M.); mataz.alcoutlabi@utrgv.edu (M.A.); Tel.: +1-956-665-3377 (J.M.); +1-956-665-8945 (M.A.)

Academic Editor: Richard Kotek
Received: 3 December 2015; Accepted: 21 May 2016; Published: 7 June 2016

Abstract: Polycaprolactone (PCL) fibers were produced using Forcespinning® (FS). The effects of PCL concentration, solvent mixture, and the spinneret rotational speed on fiber formation were evaluated. The concentration of the polymer in the solvents was a critical determinant of the solution viscosity. Lower PCL concentrations resulted in low solution viscosities with a correspondingly low fiber production rate with many beads. Bead-free fibers with high production rate and uniform fiber diameter distribution were obtained from the optimum PCL concentration (*i.e.*, 12.5 wt%) with tetrahydrofuran (THF) as the solvent. The addition of N, N-dimethylformamide (DMF) to the THF solvent promoted the gradual formation of beads, split fibers, and generally affected the distribution of fiber diameters. The crystallinity of PCL fibers was also affected by the processing conditions, spinning speed, and solvent mixture.

Keywords: fibers; centrifugal spinning; biopolymers; crystallization; DSC; electron microscopy

1. Introduction

For the past three decades, polymers have attracted considerable research attention. Polymer composites have been employed in many applications such as the construction, automotive, and petroleum industries [1,2]. The wide use of polymer composites in these industries is partly due to their relatively better properties: higher specific tensile strength, viscoelastic properties, biocompatibility, *etc*. when compared to metals and ceramics. For instance, in tissue engineering, biodegradable polymers such as PCL, poly (L-lactic acid) (PLA), polyhydroxybutyrate (PHB), and poly (glycolic acid) (PGA) are at the core of current research activities, largely due to their biodegradability and biocompatibility [3,4]. It is generally required that a biodegradable polymer have certain attributes such as stability and durability to perform the intended functions, followed by breakdown and decomposition [5,6]. The degradation of biodegradable polymers often starts from the end-groups on the polymer backbone [7]. Since the degradation begins at the end, a high surface area is common to allow for easy access to chemical and biological species [8,9]. Another feature of biodegradable polymers is that they tend not to have long chain branching. Furthermore, the polymer crosslinking often limits the number of end groups per unit molecular weight, which directly impacts the crystallinity of the polymer [10]. The low crystallinity of polymers, PCL in particular, inhibits access to the end groups, thus the biodegradability of PCL is usually attributed to the hydrolytic degradation of

the ester bonds on the polymer backbone [8]. The degradation of PCL is normally non-toxic and can further metabolize in the Krebs cycle [8]. The durability of the typical PCL polymer varies between two and four years, which sometimes is not suitable for certain applications like tissue engineering where a shorter degradation time is required. To shorten the degradation of PCL, other biodegradable polymers are often incorporated or copolymerized with it [11,12].

Nanofibers can be prepared from polymers using different processing methods including electrospinning [13], melt blowing [14], centrifugal spinning, Forcespinning® (FS) [15], liquid shearing spinning [16], touch and brush spinning [17], and most recently the reactive magnetospinning method [18,19]. The melt blowing process has been mainly developed to fabricate polyolefin fibers with a high throughput and fiber diameters ranging between several microns down to hundreds of nanometers. The production rate of melt blowing processes usually involves a linear "Exxon type" die. As such, the production rate is a function of the length of the die (e.g., 0.5 m or 1 m), the holes per inch in the die (e.g., 50 holes/inch), and the throughput per hole (e.g., 0.1, 0.4, or 1 g/hole). For example, the polymer throughput in a pilot melt blowing unit is between 0.0022 and 0.214 g/hole/min with an average fiber size ≈330 nm and a production rate of 2.23 kg/h/m of die width [14]. The fiber production rate reported here correlates to that reported by Zachary and Lozano [20] in their work on PCL fibers using the FS technique. Therefore, the fiber production rate in the melt blowing process is higher than that in the FS method. However, unlike the melt blowing process, FS does not require a high velocity of hot air to draw the fibers into the nanoscale range. Presently, the most commonly used methods for making PCL and other biocompatible polymer nanofibers include electrospinning, melt blowing, electrospray, centrifugal spinning, and recently FS. However, most of these methods can only be used to make PCL nanofibers with limited fiber production rates and thus are often restricted to lab-scale production.

The production of PCL nanofibers by electrospinning has so far been the preferred method for producing nanofibers [21–23]. However, the drawback of the electrospinning process is its limited range of materials *i.e.*, melt and solutions at higher rates. The Forcespinning® method, developed by Sarkar, Lozano, and coworkers at UTPA (now UTRGV), has been studied and proven to be suitable for the mass production of fibers from melt and solution materials for energy storage and sensor applications [24–26]. The centrifugal spinning method was originally developed by Hooper in 1924 to produce artificial silk threads from viscose or equivalent substances by applying centrifugal forces to a viscous material [27]. The centrifugal spinning method has also recently been used to produce polymer nanofibers after the pioneering work of Weitz *et al.* on the unexpected formation of nanofibers with fiber diameters in the nanometer range from a polymer solution using a standard spin-coating process [28].

It has been reported that various fiber production parameters can influence the final nanofiber properties [29]. The solvent used to dissolve the polymer usually evaporates during the spinning process and it has been shown to cause an increase in the jet viscosity of the polymer solution, which can inhibit both jet thinning and bead formation [30]. In certain applications, these beads within the fibers are considered as defects, such as in the case of scaffolds for biological tissues, where the beads may degrade cell migration and tissue genesis [30,31].

The Hansen solubility parameters have always been used as an indicator of the miscibility of a solvent with various polymers. The polymer/solvent miscibility has been shown to have a direct bearing on the final fiber diameter and morphology. For instance, fibers made from PLA in dichloromethane have been shown to have a broader range of fiber diameters [32–34]. Results reported by Wei *et al.* [35] on the electrospinning of Polyvinylidene fluoride (PVdF) nanofibers showed that the concentrations of solvent Methyl ethyl ketone (MEK) in DMF greatly influenced the dimensions and morphology of PVdF nanofibers. Kang *et al.* investigated the effect of DMF solvent on the PCL fiber formation by electrospinning PCL solutions in a co-solvents system of DCM:DMF [23]. The results showed that the low volatility of DMF led to reduced solvent evaporation, which resulted in the formation of PCL fibers that were wet at the collector plate [23]. In another study, electrospinning was

used to prepare PCL fibers from solutions with a pure DMF solvent [23]. It was found that PCL was easily separated out when DMF was used as the pure solvent, which indicated that dissolving PCL in DMF solvent resulted in a non-homogeneous solution [23]. The literature indicates that DMF has a low solubility for PCL, especially at room temperature; hence, it is considered a poor solvent for PCL [31,36]. Several studies were reported on the use of DMF solvent as an additive to other solvents such as Dichloromethane (CH_2Cl_2) and THF to enhance the electrospinnability of PCL solutions and to control the fiber morphology and structure [23,29,31,36].

The aim of this work was to investigate the formation of PCL fibers and the effects of rotational speed and solvent systems' properties on the morphology, crystallinity and thermal properties of force-spun PCL fibers. The FS experiments were carried out at different rotational speeds using different concentrations of PCL solutions. Scanning electron microscopy (SEM), differential scanning calorimetry (DSC), and X-ray diffraction (XRD) were used to characterize the morphology and structure of PCL fibers.

2. Materials and Methods

2.1. Materials

The PCL polymer with a molecular weight (M_w) of 80,000 and the solvents *N*,*N*-dimethylformamide (DMF 99.8%) and tetrahydrofuran (THF 99%) were all purchased from Sigma-Aldrich (St. Louis, MO, USA).

2.2. PCL Solution Preparation

The first batch of solutions with PCL concentrations of 7.5 wt%, 10 wt%, 12.5 wt%, 15 wt%, and 17.5 wt% were prepared by dissolving the polymer in a 50:50 by volume mixture of DMF and THF solvents. The solutions were mechanically stirred for 24 h. The purpose of this batch of solutions was to find the optimum PCL concentration that will produce fibers. A second batch was then prepared using the optimum PCL concentration (12.5 wt%) with THF as the only solvent and with varying amounts of DMF and THF; 30:70 and 40:60 by volume. This second set of solutions was meant to evaluate the effect of solvent type and mixture on fiber formation. It is worth noting that solutions consisting of the various PCL concentrations were also prepared with pure THF and pure DMF solvents. The THF–PCL solution produced similar results as the 50:50 system. On the other hand, the DMF–PCL solution produced varied results that were not consistent and not repeatable in terms of fiber production.

2.3. Forcespinning® of PCL Fibers

The fibrous mats of PCL precursors from the various solution mixtures were produced by FS. Two configurations of the FS setup can be used. A vacuum collecting system (fan collector and fiber collector) and metal bar (collectors) assembly could be employed if a large fiber mat is required to be collected (Figure 1a). If a small quantity of fibers is required, only the metal bars (collectors) can be used (Figure 1b). In such a case, microscope glass slides can be used to collect the fiber web from the collectors after they are formed (Figure 1b). In the FS technique, centrifugal forces are used to extrude a polymer solution through the spinneret. Two milliliters of the precursor solution were injected into the needle-based spinneret equipped with 30-gauge half-inch regular bevel needles. The PCL solution produced 0.32 g of fibers in 2 min, compared to less than 0.1 g/h produced when using a typical lab scale electrospinning system. The rotational speed of the spinneret was varied at 1000–10,000 rpm for a spinning time of 2 min. The substrate (fan collector) was rotated 90° and the needles were changed after each run. The PCL fibrous mats were removed from the vacuum collecting system and were covered and stored under desiccation prior to being characterized.

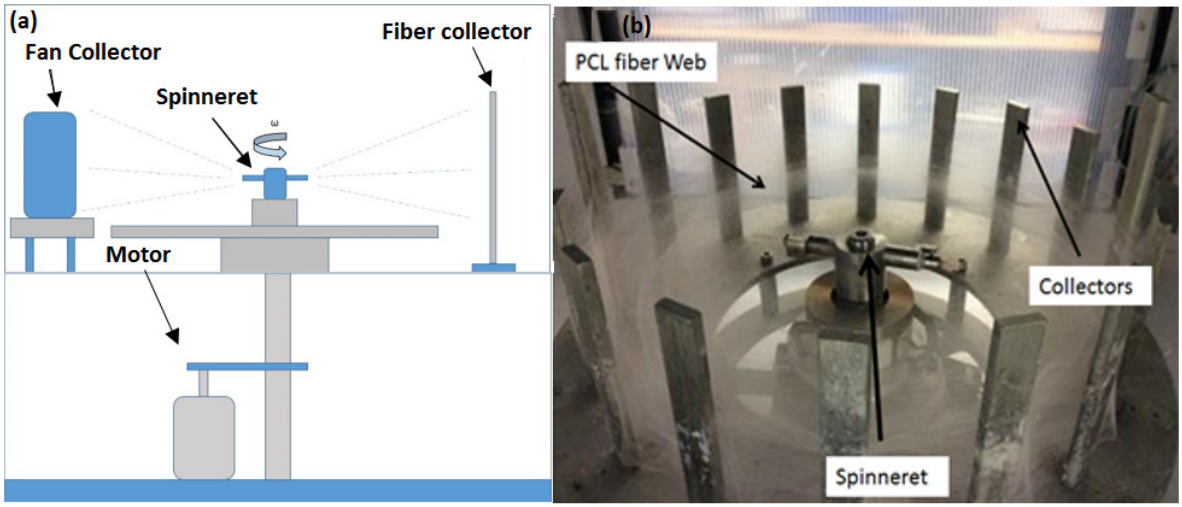

Figure 1. (**a**) Schematic diagram of the FS method and (**b**) digital photo showing the fiber web, spinneret, and collector setup.

2.4. Fiber Characterization

2.4.1. Scanning Electron Microscopy

The morphologies of the samples were investigated with a field emission scanning electron microscope, SEM-Zeiss (Carl Zeiss AG, Oberkochen, Germany). The samples were coated with a thin layer of silver–palladium for 180 s at 45 mA with a Desk II Denton Vacuum Cold Sputter prior to imaging. The digital micrograph software GATAN (Gatan Inc., Pleasanton, CA, USA) was used to determine the average fiber diameter of the force-spun PCL fibers. To obtain statistically reliable data, five to seven SEM micrographs from different parts of a 0.5 cm × 0.5 cm sample area were taken and used to collect/measure the fiber diameters and generate histograms to show the fiber diameter distribution. In the GATAN software, an average of 85 fibers from the SEM micrographs were used and one diameter measurement was taken from each individual fiber.

2.4.2. X-Ray Diffraction

The X-ray diffraction spectra of the prepared PCL fibers were analyzed in a Bruker 800D X-ray diffractometer with CuKα_1 radiation (λ = 0.15406 nm, Bruker Cop, Billerica, MA, USA). The XRD data was collected by using a scanning mode in the 2θ ranging from 10° to 80° with a scanning step size of 0.02° and a scanning rate of 0.1° min^{-1}.

2.4.3. Differential Scanning Calorimetry (DSC)

The thermal properties of the PCL fibers were evaluated using a TA-Q series 60 DSC (TA Instruments, New Castle, DE, USA). The DSC thermograms were obtained at a heating rate of 10 °C/min to 180 °C, followed by cooling to 30 °C at 10 °C/min, and then a second heating to 180 °C was performed at the same rate. The melting temperature (T_m) and enthalpy (ΔH_m) were then obtained from the melting endotherm peak. The crystallization temperature (T_c) at the exothermic peak and crystallization enthalpy (ΔH_c) were determined during the cooling process of the PCL samples. The crystallinity of the PCL fibers was determined from the experimental heat of fusion obtained by integrating the peaks and using a baseline enthalpy of fusion value of 139.5 J/g for a 100% crystalline PCL sample.

3. Results and Discussion

3.1. PCL Fiber Surface Characterization: SEM Analysis

The force-spun fibers prepared from PCL solutions with lower concentrations (*i.e.*, 7.5 wt%, 10 wt%) in a DMF:THF mixture (50:50 by volume) showed a significant number of beads but sparse fibers, as shown in Figure 2a–c and the supplementary data sheets (Table S1, Figures S1 and S2). On the other hand, increasing the PCL concentration to 15 wt% and 17.5 wt% resulted in the formation of beads and fibers. It can be seen in the supplementary data sheet (Figures S3 and Figure S4) that fibers were formed with the use of 15 wt% PCL at 7000–8000 rpm and 17.5 wt% PCL at 5000–9000 rpm. The Forcespinning of 15 wt% PCL solutions at 6000, 9000, and 10,000 rpm resulted in the formation of beads and a few fibers (Figure S3). At these higher concentrations of PCL (*i.e.*, 15 wt% and 17.5 wt%), needle clogging was observed 30 s after starting the FS experiment. The centrifugal forces in this case were not enough to extrude the solution, so very few fibers were produced. However, at a higher rotational speed of 10,000 rpm, the highly viscous solution produced thicker fibers, albeit some beads formed due to limited fiber elongation, as shown in Figure 2e,f. It can be observed that at a PCL concentration of 12.5 wt% and solvent concentration of 50:50 in the DMF:THF mixture, a substantial number of fibers were produced but an insignificant number of beads (Figure 3); there was a typical fiber diameter distribution ranging from 2 μm to 4 μm, as shown in Figure 3a insert. This PCL concentration was thus considered the optimum value.

Rotational speeds lower than 3000 rpm were insufficient to eject all the solution from the spinneret, resulting in no fiber formation. However, for a PCL concentration of 10 wt%, a substantial number of fibers was formed with a significant number of beads (Figure S2), thus the rotational speed had a direct effect on fiber production. Spinneret rotational speeds above 8000 rpm produced fibers with many beads regardless of the concentration of PCL or the solvent mixture, as seen in the supplementary data sheet. The formation of beaded fibers is caused by the shortened solidification time between the ejections of the polymer solution (in the form of a droplet) from the spinneret to its deposition on the substrate. With a PCL concentration of 12.5 wt%, spinneret rotational speeds between 5000 and 8000 rpm produced PCL fibers without beads. This range of rotational speeds enabled the polymer jet to elongate and travel in a spiral trajectory towards the vacuum collecting system while the solvent evaporated to form continuous PCL fibers.

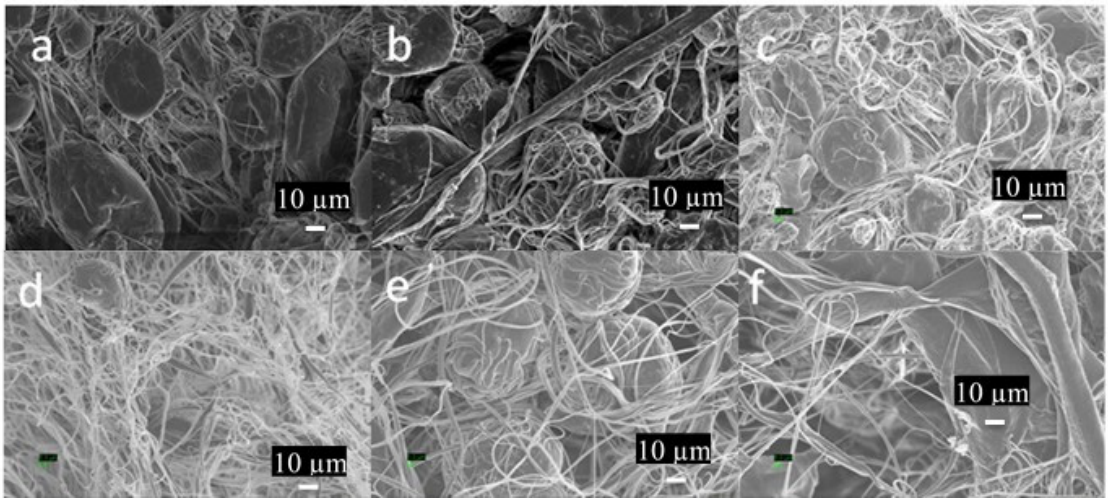

Figure 2. SEM images of PCL fibers prepared with THF as the only solvent with different PCL concentrations using different rotational speeds. (**a**) PCL 7.5 wt% at 4000 rpm; (**b**) PCL 7.5 wt% at 10,000 rpm; (**c**) PCL 10 wt% at 4000 rpm; (**d**) PCL 10 wt% at 8000 rpm; (**e**) PCL 15 wt% at 10,000 rpm; (**f**) PCL 17.5 wt% at 10,000 rpm.

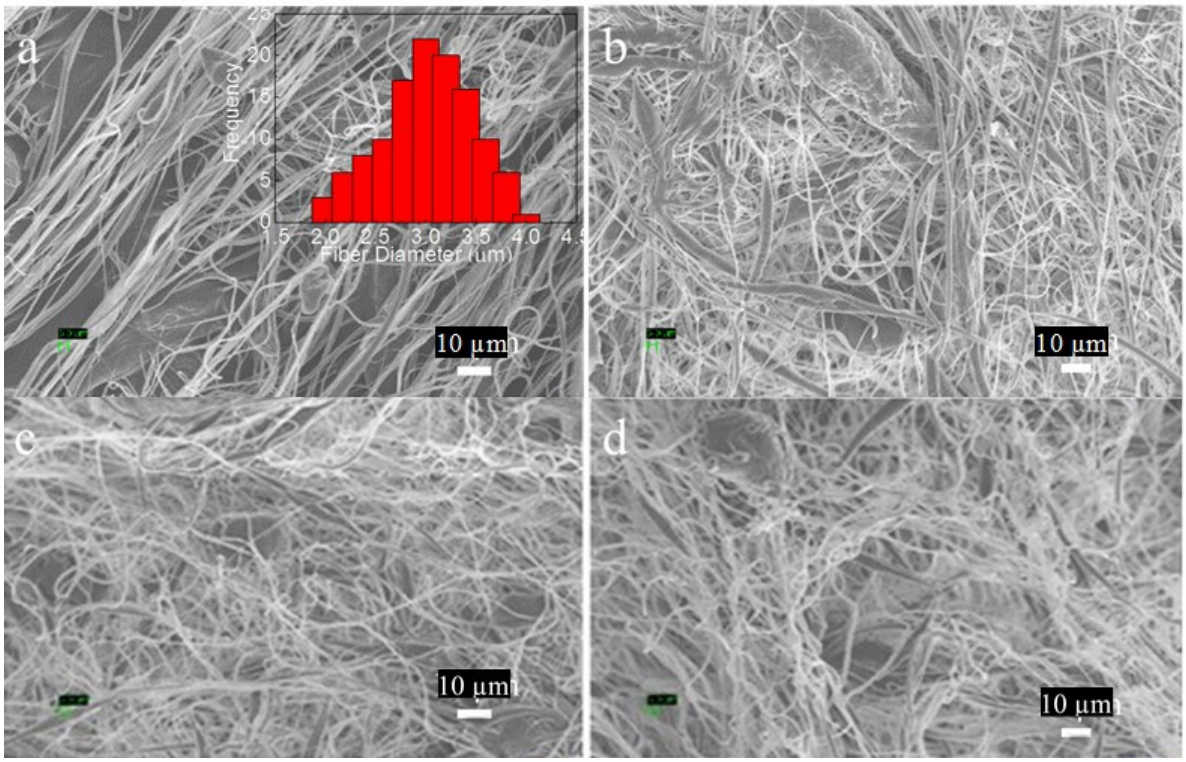

Figure 3. SEM images of PCL fibers prepared from 12.5 wt% PCL in solvent ratios of 50:50 (DMF:THF) mixtures and at different rotational speeds. (**a**) 5000 rpm; (**b**) 6000 rpm; (**c**) 7000 rpm; (**d**) 8000 rpm with a typical fiber diameter distribution in insert (**a**).

The fibers produced from THF solvent only in 12.5 wt% PCL concentration showed bead-free uniform fibers, as shown in Figure 4. There was also a noticeable change in the fiber diameter as a function of the rotational speed of the spinneret (Figure 5). As the rotational speed increased from 7000 and 8000 rpm, a significant number of fibers, with a fiber diameter in the range of 3 µm and 4 µm, formed. The lower speeds produced fibers with a diameter in the 250 nm–1 µm range (Figure 5). The histograms of corresponding fiber diameter clearly showed that more uniform fibers were obtained at lower spinning speeds. As the spinning speeds increased from 5000 to 8000 rpm, the average fiber diameter increased from 0.25 to 2.04 µm. These changes in fiber morphology and size distribution were attributed to the changes in spinneret rotational speeds during the FS process.

The SEM images for the different solvent mixtures of DMF and THF in 12.5 wt% PCL (30:70 and 40:60 by volume) are shown in Figures 6 and 7, respectively. The corresponding diameter distribution analyses are shown in Figures 8 and 9, respectively. With the addition of the DMF solvent, the surface morphology of the PCL fibers from the SEM micrographs showed some noticeable changes in fiber morphology and diameter distribution. There was some variation in fiber diameter distribution when compared to the fibers produced from PCL in 100% THF solvent (Figure 5 *vs*. Figure 8 or Figure 9). In addition, a small quantity of beads and split fibers were observed when the ratio of the THF solvent increased from 40:60 (DMF:THF) to 30:70, as shown in Figures 6 and 8 *vs*. Figures 7 and 9. The bead content in the fibers remarkably increased at higher rotational speeds, as shown in the supplementary data sheet (Figure S5, Table S2 and Figure S6 (g and h)). These observations further suggest that the addition of DMF solvent and the rotational speed had a substantial effect on the fiber formation and morphology. These results further indicated that the addition of DMF promoted the gradual formation of beads and split fibers, and generally affected the distribution of fiber diameters. The explanation for this observed trend is that the THF solvent with higher vapor pressure (*i.e.*, 20 kPa at 20 °C) is more likely to evaporate during the FS process than the DMF with a lower vapor pressure (0.5 kPa at 20 °C). For PCL/THF solutions, the rapid evaporation of THF solvent led to incomplete crystallization of the

formed fibers, thus the PCL macromolecules did not have enough time to align and pack under this condition. This indicates that less toxic solvents such as DMF and THF can be used to produce PCL fibers of equal quality when compared to those produced using other relatively toxic solvents such as dichloromethane [20].

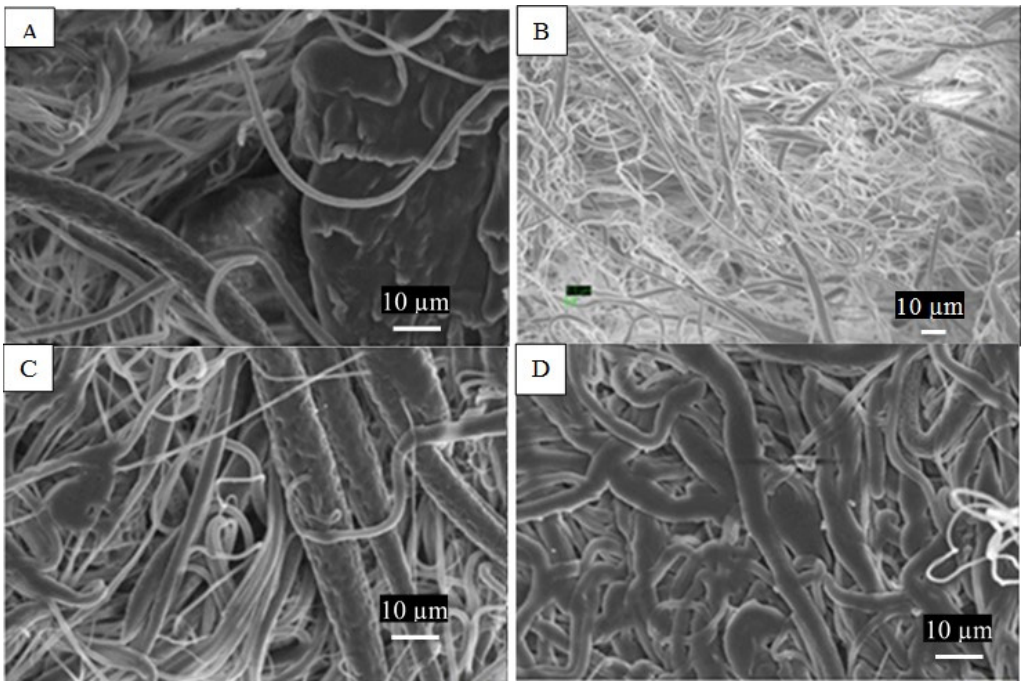

Figure 4. SEM images of PCL fibers prepared from 12.5 wt% PCL in THF solvent only, at different rotational speeds. (**A**) 5000 rpm; (**B**) 6000 rpm; (**C**) 7000 rpm; (**D**) 8000 rpm.

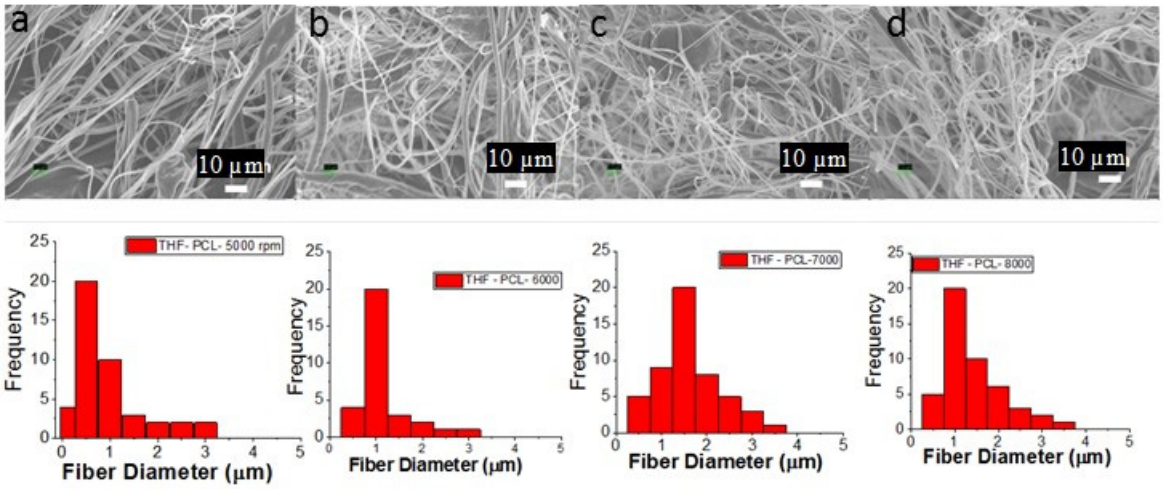

Figure 5. SEM images of PCL fibers prepared from 12.5 wt% PCL in THF as the solvent at different rotational speeds. (**a**) 5000 rpm; (**b**) 6000 rpm; (**c**) 7000 rpm; (**d**) 8000 rpm and corresponding histograms of the fiber diameter.

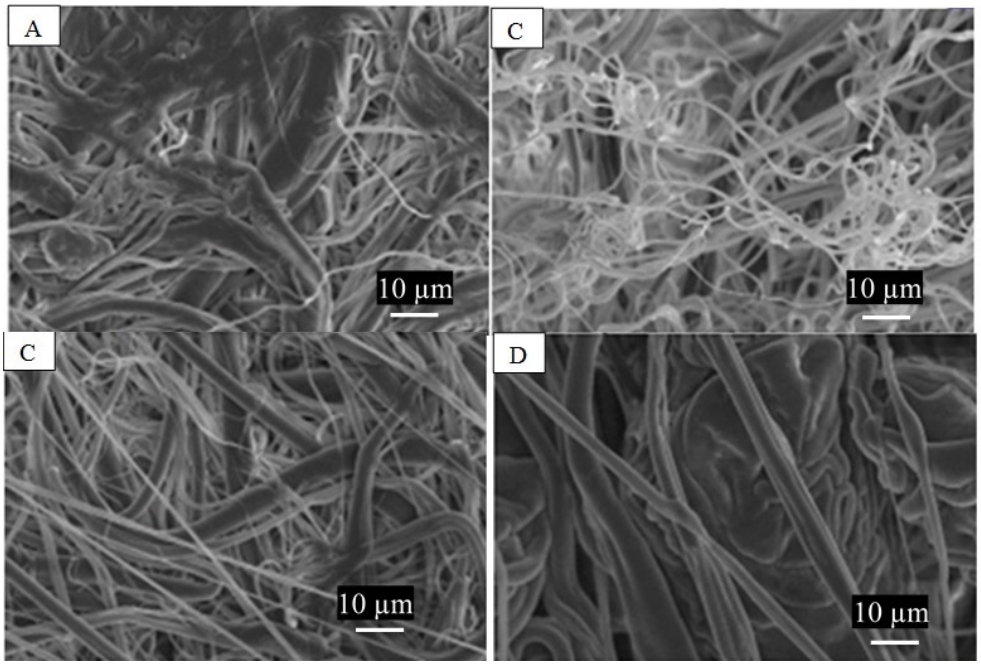

Figure 6. SEM images of PCL fibers prepared from 12.5 wt% PCL solutions in solvent ratios of 30:70 (DMF:THF) mixtures and at different rotational speeds. (**A**) 5000 rpm; (**B**) 6000 rpm; (**C**) 7000 rpm; (**D**) 8000 rpm.

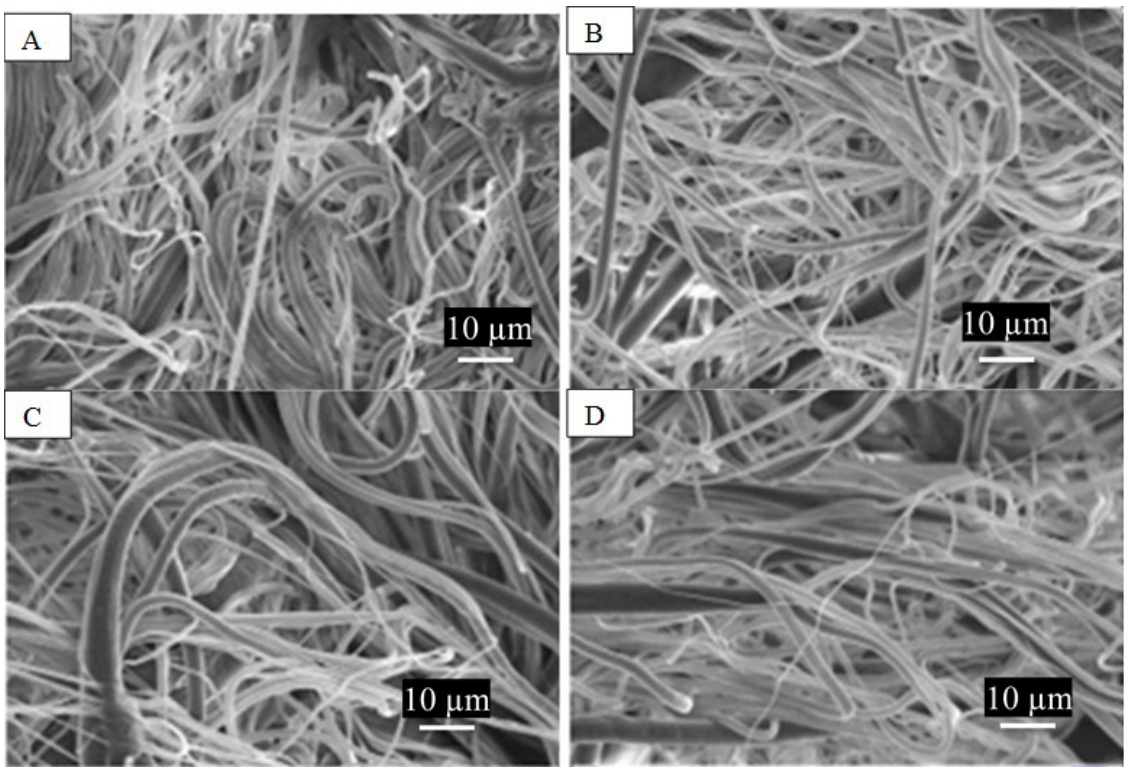

Figure 7. SEM images of PCL fibers prepared from 12.5 wt% PCL solutions in solvent ratios of 40:60 (DMF:THF) mixtures and at different rotational speeds. (**A**) DMF:THF (40:60) at 5000 rpm; (**B**) DMF:HF (40:60) at 6000 rpm; (**C**) DMF:THF (40:60) at 7000 rpm; (**D**) DMF:THF (40:60) at 8000 rpm.

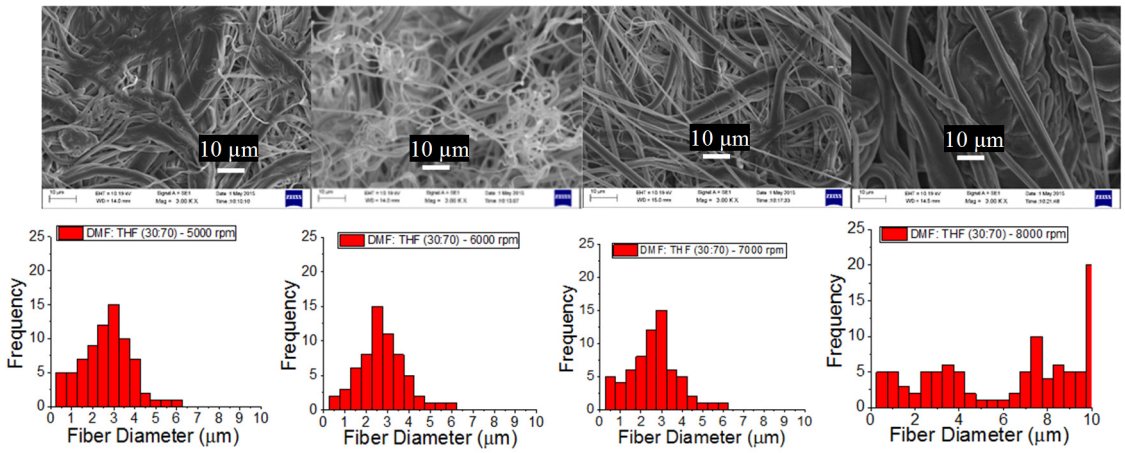

Figure 8. SEM images of the PCL fibers from solvent ratio 30:70 of DMF:THF mixture at different rotational speeds used, (**a**) 5000 rpm; (**b**) 6000 rpm; (**c**) 7000 rpm; (**d**) 8000 rpm and corresponding histogram of the fiber diameters.

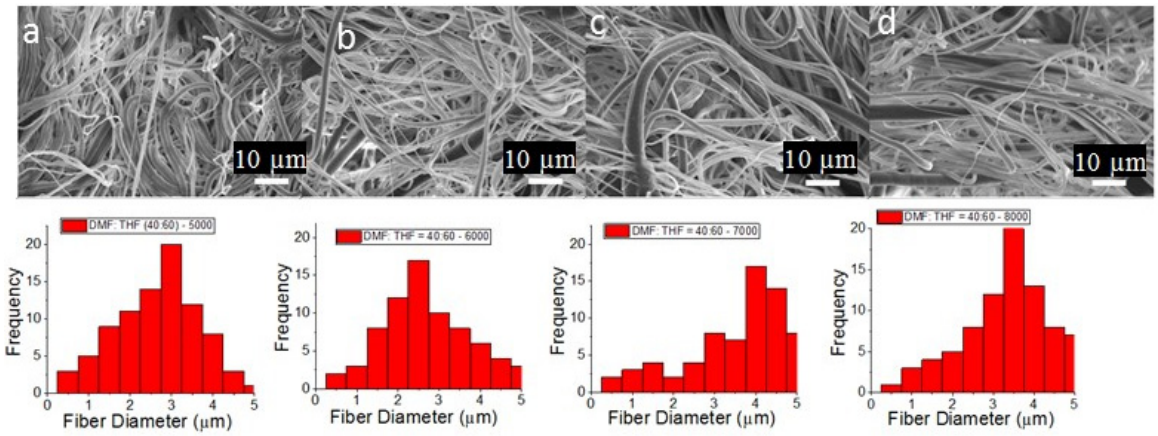

Figure 9. SEM images of the -prepared samples of the PCL fibers with solvent ratios of DMF:THF at 40:60 and at different rotational speeds used, (**a**) 5000 rpm; (**b**) 6000 rpm; (**c**) 7000 rpm; (**d**) 8000 rpm and corresponding histogram of the fiber diameter.

3.2. XRD Analysis

The XRD patterns for the PCL fibers produced from various solvent mixtures in 12.5 wt% PCL are shown in Figure 10a–c. There were two major peaks from the polymer represented at 2θ = 21.36° and 23.87°, with a shoulder at 22.1°. The two peaks at 2θ = 21.36° and 23.87° were indexed to be (110) and (200) crystallographic planes. The sharpness of these major peaks indicates the semi-crystalline nature of the PCL. The observed crystallinity in PCL fibers was attributed to the mechanical forces that stretched the fibers, thereby aligning the macromolecules of the polymer as they came out of the spinneret.

The X-ray spectra of the PCL fibers produced from 100% THF solvent (Figure 10a) showed much lower full width at half maximum (FWHM) values for the two prominent peaks at 2θ = 21.36° and 23.87° relative to those of fibers from different solvent ratios of DMF:THF. In addition, the relative sharpness of the peaks was a function of the spinning speed as well as the solvent mixture, *i.e.*, peak sharpness decreases as spinning speed decreases. For instance, it can be observed that the XRD patterns of the fibers obtained with DMF:THF solvent ratio (40:60 per volume) showed very weak peaks at 5000 rpm (Figure 10c), while that of solvent ratio 30:70 at the same rotational speed showed no peak at all (Figure 10b). Thus, these results suggest that the crystallinity of the PCL did not follow any trend as far as the addition of DMF solvent along with THF goes. It was expected that a higher amount of the

THF solvent in (DMF:THF) mixture would not significantly reduce the formation of crystalline regions in PCL fibers at lower rotational speeds since PCL fibers produced from 12.5 wt% PCL/THF solution showed peaks at a rotational speed of 5000 rpm (Figure 10a *vs.* Figure 10c). This observed trend could not be readily explained.

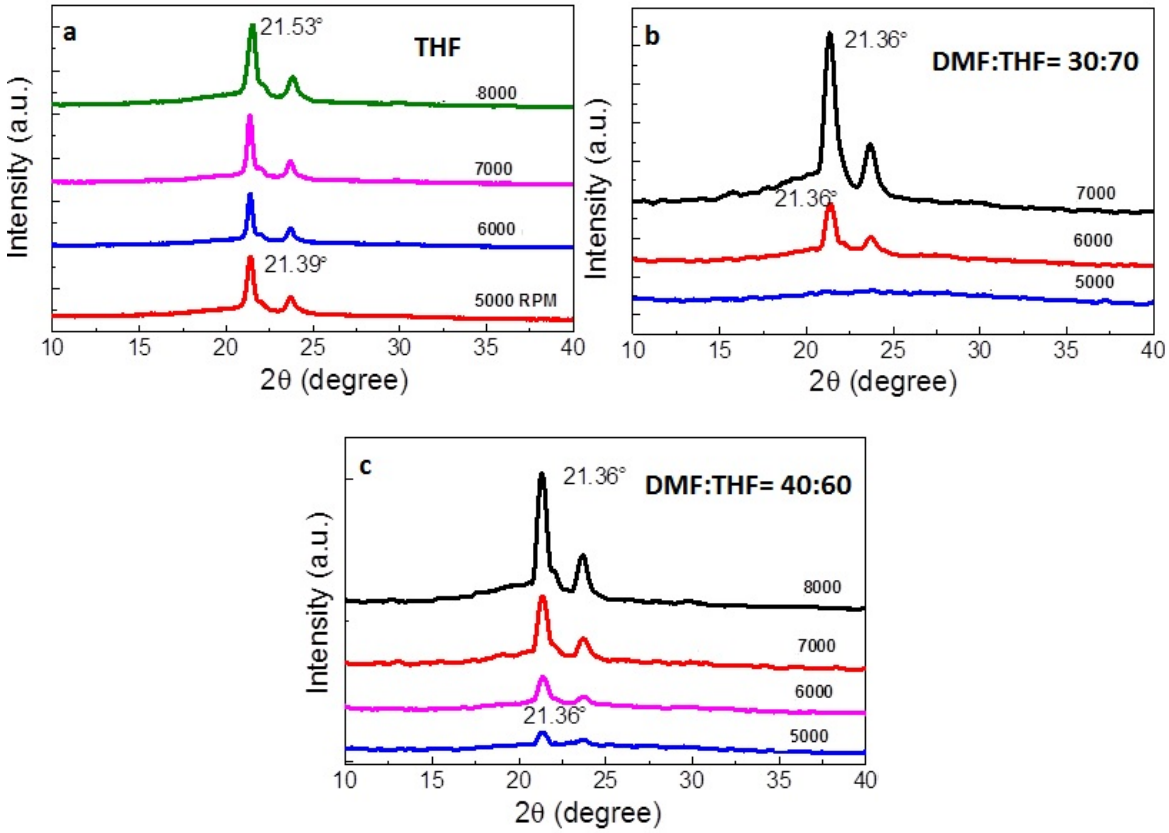

Figure 10. XRD patterns of PCL fibers obtained by FS at different rotational speeds and concentration of PCL solutions, and different solvent mixtures: (**a**) 100% THF solvent; (**b**) 30:70 solvent ratio of DMF:THF; (**c**) 40:60 solvent ratio of DMF:THF.

3.3. DSC Results

The thermal properties and crystallinity of PCL fibers were evaluated from the DSC endotherms in Figures 11–13. These results were determined for the different DMF:THF solvent mixture mixtures and spinning speeds. The enthalpy (ΔH_m), melting (T_m), and crystallization (T_c) temperatures were measured from the first and second heating cycles of DSC endotherms, as illustrated in Table 1. These thermal properties of the PCL fibers demonstrate that the melting temperature (T_m) of the produced fibers was independent or varied slightly with the solvent mixture (*i.e.*, DMF:THF ratios of 40:60, 30:70, and 0:100) as well as the rotational speed for the fiber production process. The crystallinity was calculated using the following equation:

$$X_c = \frac{\Delta H_m - \Delta H_c}{\Delta H_f},$$

where ΔH_m is the enthalpy of fusion, ΔH_c is the enthalpy of cold crystallization, and ΔH_f is the enthalpy of fusion of a 100% crystalline sample (139.5 J$\cdot$ g^{-1}).

Although not significant, the DSC results (Table 1) showed some variations in the crystallization temperature (T_c). The values of the exothermic enthalpy (ΔH_c) were higher for PCL fibers prepared at lower rotational speeds and higher THF concentrations. However, Table 1 shows inconsistent results for PCL fibers produced at varied rotational speeds with only THF as the solvent. Nevertheless,

these results showed that fibers with lower crystallinity (0.02–0.11) were produced after the addition of the non-volatile solvent DMF to THF (40:60) when compared to those formed with 100% THF solvent. The temperature at the peak of crystallization (T_c) for the PCL fibers varies slightly with the solvent mixture and the spinneret rotational speed. The observed trend was consistent with the XRD results.

Table 1. DSC results of bulk PCL and fibers prepared by Forcespinning®.

DMF:THF	Spinneret Speed	First Heating		Second Heating		Cooling		
		ΔH_m (J/g)	ΔT_m (°C)	ΔH_m (J/g)	ΔT_m (°C)	ΔH_c (J/g)	ΔT_c (°C)	Crystallinity
PCL (Bulk)	–	60.4	65.9	48.6	58.4	30.1	31.7	0.22
00:100	5000	56.9	63.3	49.2	58.4	43.9	34.5	0.1
	6000	52.5	66.2	42.8	59.9	35.6	34.4	0.12
	7000	51.9	62.5	45	58.1	43.3	36	0.1
	8000	62.4	63.3	45.5	61.5	45.5	35.8	0.12
30:70	5000	66.9	64.3	56	59.4	50.9	35.4	0.12
	6000	73.3	64.2	52.6	58.8	46.9	35.8	0.19
	7000	52.1	65	51.9	59.6	48.5	34.5	0.1
	8000	71	64.6	51.7	57.3	46.7	35.3	0.2
40:60	5000	49.8	64.3	48.2	58.6	44	35.2	0.04
	6000	64.4	64.1	49.2	59.4	49	35.9	0.11
	7000	53.2	64.2	41.4	60.1	40.6	36.1	0.1
	8000	46.7	64.6	43.6	60.2	43.5	35.5	0.02

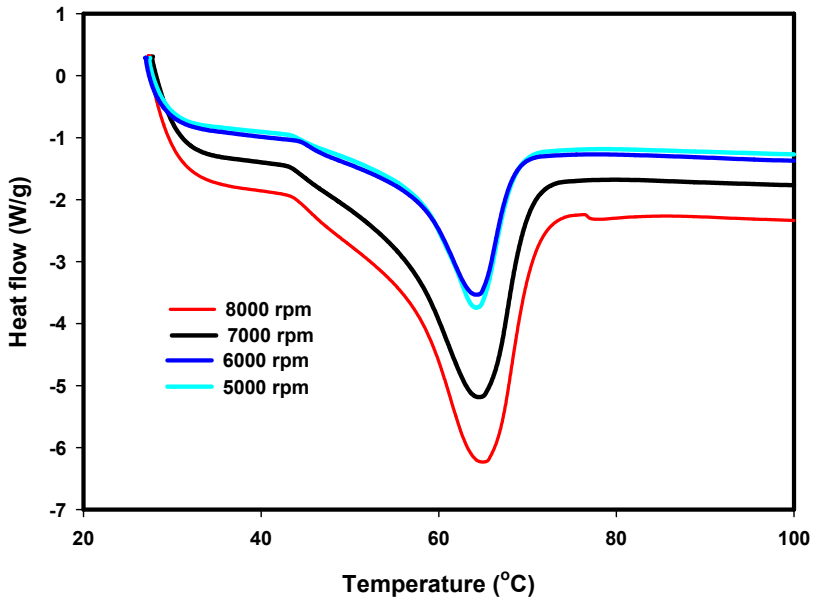

Figure 11. Melting endotherm of PCL fibers prepared by the FS of 12.5 wt% PCL solutions in DMF:THF (30:70 by volume) mixture at different rotational speeds.

The values of the enthalpy of fusion calculated from the first endothermic heating process were much higher than for the second endothermic heating. Furthermore, the PCL fibers made from different solvent mixtures had a lower crystallinity than that of the bulk PCL material, because the PCL fibers' crystallization process was incomplete relative to the bulk material. This observed trend was probably due to the formation of a second crystalline phase prior to the main crystallization as a result of stress-induced crystallization during processing [37]. This is consistent with the results reported in the literature for PCL [20] and nylon fibers [38].

Finally, it can be observed (Table 1) that higher ratios of DMF in the solvent mixture (*i.e.*, 30:70 of DMF:THF) produced PCL fibers with higher crystallinity compared to those prepared from PCL solutions in THF solvent only. In the light of this, future work is needed to investigate the solvent volatility and its effect on the crystallization of force-spun fibers.

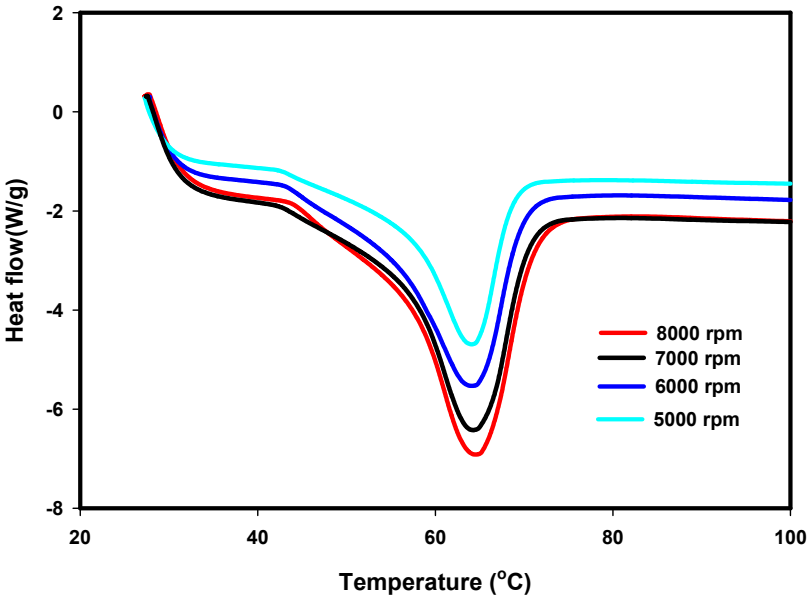

Figure 12. Melting endotherm of PCL fibers prepared by the FS of 12.5 wt% PCL solutions in DMF:THF (40:60 by volume) mixture at different rotational speeds.

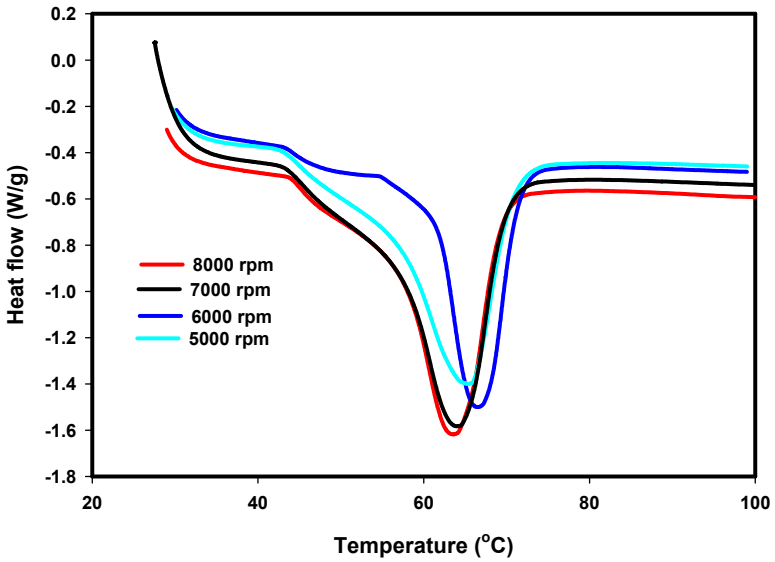

Figure 13. Melting endotherm of PCL fibers prepared by the Forcespinning® of 12.5 wt% PCL/THF solutions at different rotational speeds.

Additional DSC experiments were performed on the PCL fibers to ensure that this secondary crystallization peak, which appears only after the FS of PCL fibers, was only due to processing and not to the solvent mixture. Figure 14 shows the DSC scan of PCL fibers with two different solvent mixtures of DMF:THF ratios (0:100 and 30:70 by volume) and at a rotational speed of 5000 rpm, obtained at the first and second heating scans. The results shown in Figure 14 clearly demonstrate that the second crystallization peak observed after processing (stress-induced crystallization) disappeared after

the second DSC heating scan. The heating–cooling peaks also showed that the endotherm melting transition of PCL fibers exhibited a sharp transition peak without any manifestation of a secondary crystallization. This phenomenon was observed for all the PCL fibers produced from the different solvent mixtures. This second DSC result also reaffirms that the crystallinity of the PCL fibers was attributed to the centrifugal forces that stretched and aligned the macromolecules of the fibers as they come out of the spinneret.

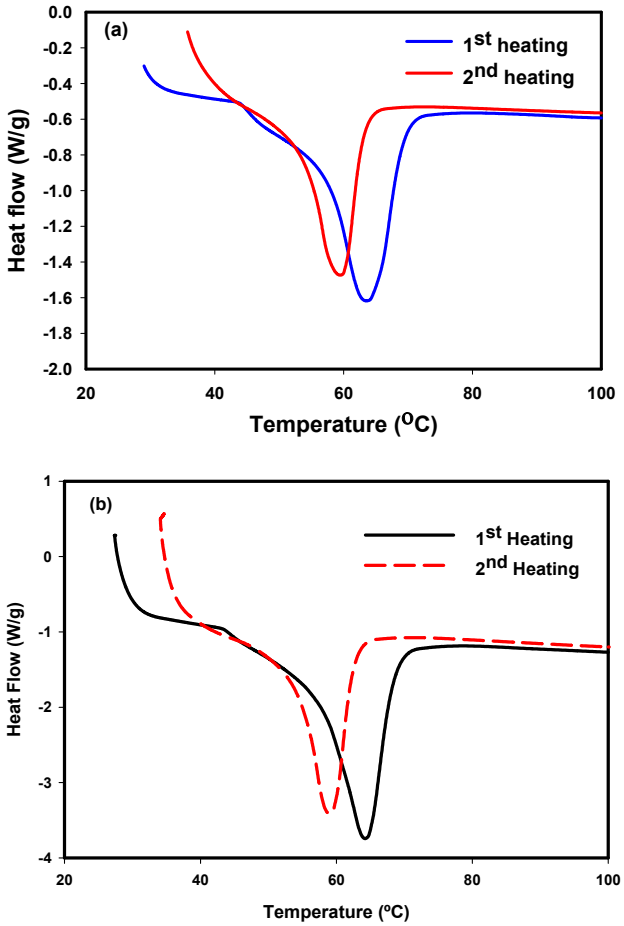

Figure 14. Melting endotherms at the first and second heating scans of PCL fibers prepared by Forcespinning® of 12.5 wt% PCL solutions in in DMF:THF (**a**) (0:100) and (**b**) (30:70) mixtures at a rotational speed of 5000 rpm. The secondary crystallization process disappeared after the second DSC heating scan for both samples.

4. Conclusions

To produce highly crystalline, uniform fiber diameter distribution and bead-free PCL fibers, the critical determinant factors were the PCL concentration, solvent mixture, and the rotational speed. No beads, a higher fiber production rate, and uniform fiber diameter distribution were obtained with an optimum PCL concentration of 12.5 wt% with only THF as the solvent. The addition of DMF as a solvent promoted the gradual formation of beads and split fibers, and generally affected the distribution of fiber diameters. The crystallinity of PCL fibers was also affected by processing conditions such as spinning speed and solvent mixture.

Supplementary Materials: Figures S1–S6 and Tables S1–S2 can be accessed at: http://www.mdpi.com/2079-6439/4/2/20/s1.

Acknowledgments: This research was supported by NSF PREM with award number DMR-1523577. Partial funding was also received from the following agencies: the USDA, the National Institute of Food and

Agriculture, and the Integrating Food Science/Engineering and Education Network (IFSEEN) with award number: 2015-38422-24059.

Author Contributions: Nancy Obregon, Howard Campos, David De la Garza and David Flores conducted most the experiments in this work regarding solution preparation, Forcespinning and SEM sample preparation. Howard Campos and Victor Agubra carried out the DSC experiments and analyzed the results. Madhab Pokhrel and Yuanbing Mao conducted the XRD and SEM experiments and analyzed the SEM and XRD results. Victor Agubra, Madhab Pokhrel, Javier Macossay and Mataz Alcoutlabi wrote and finalized the manuscript.

Conflicts of Interest: The authors declare no conflict of interest.

References

1. Mohammed, L.; Ansari, M.N.M.; Pua, G.; Jawaid, M.; Islam, M.S. A review on natural fiber reinforced polymer composite and its applications. *Int. J. Polym. Sci.* **2015**, *2015*, 243947:1–243947:15. [CrossRef]
2. Xu, X.; Jayaraman, K.; Morin, C.; Pecqueux, N. Life cycle assessment of wood-fibre-reinforced polypropylene composites. *J. Mater. Process. Technol.* **2008**, *198*, 168–177. [CrossRef]
3. Zhou, L.; Zhao, G.; Feng, Y.; Yin, J.; Jiang, W. Toughening polylactide with polyether-block-amide and thermoplastic starch acetate: Influence of starch esterification degree. *Carbohydr. Polym.* **2015**, *127*, 79–85. [CrossRef] [PubMed]
4. Tallawi, M.; Rosellini, E.; Barbani, N.; Cascone, M.G.; Rai, R.; Saint-Pierre, G.; Boccaccini, A.R. Strategies for the chemical and biological functionalization of scaffolds for cardiac tissue engineering: A review. *J. R. Soc. Interface* **2015**, *12*. [CrossRef] [PubMed]
5. Becker, J.; Lu, L.; Runge, M.B.; Zeng, H.; Yaszemski, M.J.; Dadsetan, M. Nanocomposite bone scaffolds based on biodegradable polymers and hydroxyapatite. *J. Biomed. Mater. Res. Part A* **2015**, *103*, 2549–2557. [CrossRef] [PubMed]
6. Cho, D.I.D.; Yoo, H.J. Microfabrication methods for biodegradable polymeric carriers for drug delivery system applications: A review. *J. Microelectromech. Syst.* **2015**, *24*, 10–18. [CrossRef]
7. Colwell, J.M.; Wentrup-Byrne, E.; George, G.A.; Schue, F. A pragmatic calcium-based initiator for the synthesis of polycaprolactone copolymers. *Polym. Int.* **2015**, *64*, 654–660. [CrossRef]
8. Woodruff, M.A.; Hutmacher, D.W. The return of a forgotten polymer—Polycaprolactone in the 21st century. *Progr. Polym. Sci.* **2010**, *35*, 1217–1256. [CrossRef]
9. Yazdimamaghani, M.; Razavi, M.; Vashaee, D.; Pothineni, V.R.; Rajadas, J.; Tayebi, L. Significant degradability enhancement in multilayer coating of polycaprolactone-bioactive glass/gelatin-bioactive glass on magnesium scaffold for tissue engineering applications. *Appl. Surf. Sci.* **2015**, *338*, 137–145. [CrossRef]
10. Makhijani, K.; Kumar, R.; Sharma, S.K. Biodegradability of blended polymers: A comparison of various properties. *Crit. Rev. Environ. Sci. Technol.* **2015**, *45*, 1801–1825. [CrossRef]
11. Belkhir, K.; Shen, H.; Chen, J.; Jegat, C.; Taha, M. Synthesis of multi-thiol functionalized polylactic acid, polyhydroxybutyrate and polycaprolactone. *Eur. Polym. J.* **2015**, *66*, 290–300. [CrossRef]
12. Oh, H.-K.; Lee, H.S.; Lee, J.H.; Oh, S.H.; Lim, J.-Y.; Ahn, S.; Hwang, J.-Y.; Kang, S.-B. Functional and histological evidence for the targeted therapy using biocompatible polycaprolactone beads and autologous myoblasts in a dog model of fecal incontinence. *Dis. Colon Rectum* **2015**, *58*, 517–525. [CrossRef] [PubMed]
13. Li, D.; Xia, Y.N. Electrospinning of nanofibers: Reinventing the wheel? *Adv. Mater.* **2004**, *16*, 1151–1170. [CrossRef]
14. Hassan, M.A.; Yeom, B.Y.; Wilkie, A.; Pourdeyhimi, B.; Khan, S.A. Fabrication of nanofiber meltblown membranes and their filtration properties. *J. Membr. Sci.* **2013**, *427*, 336–344. [CrossRef]
15. Agubra, V.A.; De la Garza, D.; Gallegos, L.; Alcoutlabi, M. Forcespinning of polyacrylonitrile for mass production of lithium-ion battery separators. *J. Appl. Polym. Sci.* **2016**, *133*. [CrossRef]
16. Smoukov, S.K.; Tian, T.; Vitchuli, N.; Gangwal, S.; Geisen, P.; Wright, M.; Shim, E.; Marquez, M.; Fowler, J.; Velev, O.D. Scalable liquid shear-driven fabrication of polymer nanofibers. *Adv. Mater.* **2015**, *27*, 2642–2647. [CrossRef] [PubMed]
17. Tokarev, A.; Asheghali, D.; Ian, M.; Griffiths, I.M.; Trotsenko, O.; Gruzd, A.; Lin, X.; Stone, H.A.; Minko, S. Touch- and brush-spinning of nanofibers. *Adv. Mater.* **2015**, *27*, 6526–6532. [CrossRef] [PubMed]
18. Tokarev, A.; Trotsenko, O.; Griffiths, I.M.; Stone, H.A.; Minko, S. Magnetospinning of nano- and microfibers. *Adv. Mater.* **2015**, *27*, 3560–3565. [CrossRef] [PubMed]

19. Tokarev, A.T.; Asheghali, D.; Griffiths, I.M.; Stone, H.A.; Minko, S. Reactive magnetospinning of nano- and microfibers. In *Angewandte Chemie (International ed. in English)*; WILEY-V C H VERLAG GMB: Weinheim, Germany, 2015; Volume 54, pp. 13613–13616.
20. McEachin, Z.; Lozano, K. Production and characterization of polycaprolactone nanofibers via forcespinning (TM) technology. *J. Appl. Polym. Sci.* **2012**, *126*, 473–479. [CrossRef]
21. He, M.; Xue, J.; Geng, H.; Gu, H.; Chen, D.; Shi, R.; Zhang, L. Fibrous guided tissue regeneration membrane loaded with anti-inflammatory agent prepared by coaxial electrospinning for the purpose of controlled release. *Appl. Surf. Sci.* **2015**, *335*, 121–129. [CrossRef]
22. Zhang, Q.; Lv, S.; Lu, J.; Jiang, S.; Lin, L. Characterization of polycaprolactone/collagen fibrous scaffolds by electrospinning and their bioactivity. *Int. J. Biol. Macromol.* **2015**, *76*, 94–101. [CrossRef] [PubMed]
23. Doustgani, A. Effect of electrospinning process parameters of polycaprolactone and nanohydroxyapatite nanocomposite nanofibers. *Text Res. J.* **2015**, *85*, 1445–1454. [CrossRef]
24. Weng, B.C.; Xu, F.H.; Garza, G.; Alcoutlabi, M.; Salinas, A.; Lozano, K. The production of carbon nanotube reinforced poly(vinyl) butyral nanofibers by the forcespinning (R) method. *Polym. Eng. Sci.* **2015**, *55*, 81–87. [CrossRef]
25. Sarkar, K.; Gomez, C.; Zambrano, S.; Ramirez, M.; de Hoyos, E.; Vasquez, H.; Lozano, K. Electrospinning to forcespinning™. *Mater. Today* **2010**, *13*, 12–14. [CrossRef]
26. Weng, B.C.; Xu, F.H.; Alcoutlabi, M.; Mao, Y.B.; Lozano, K. Fibrous cellulose membrane mass produced via forcespinning® for lithium-ion battery separators. *Cellulose* **2015**, *22*, 1311–1320. [CrossRef]
27. Hooper, J.P. Centrifugal Spinneret. US 1500931 A, 8 July 1924.
28. Weitz, R.T.; Harnau, L.; Rauschenbach, S.; Burghard, M.; Kern, K. Polymer nanofibers via nozzle-free centrifugal spinning. *Nano Lett.* **2008**, *8*, 1187–1191. [CrossRef] [PubMed]
29. Fong, H.; Chun, I.; Reneker, D.H. Beaded nanofibers formed during electrospinning. *Polymer* **1999**, *40*, 4585–4592. [CrossRef]
30. Golecki, H.M.; Yuan, H.Y.; Glavin, C.; Potter, B.; Badrossamay, M.R.; Goss, J.A.; Phillips, M.D.; Parker, K.K. Effect of solvent evaporation on fiber morphology in rotary jet spinning. *Langmuir* **2014**, *30*, 13369–13374. [CrossRef] [PubMed]
31. Ruder, W.C.; Pratt, E.D.; Bakhru, S.; Sitti, M.; Zappe, S.; Cheng, C.M.; Antaki, J.F.; LeDuc, P.R. Three-dimensional microfiber devices that mimic physiological environments to probe cell mechanics and signaling. *Lab Chip* **2012**, *12*, 1775–1779. [CrossRef] [PubMed]
32. Ali Akbari Ghavimi, S.; Ebrahimzadeh, M.H.; Solati-Hashjin, M.; Abu Osman, N.A. Polycaprolactone/starch composite: Fabrication, structure, properties, and applications. *J. Biomed. Mater. Res. Part A* **2015**, *103*, 2482–2498. [CrossRef] [PubMed]
33. Gonen, S.O.; Taygun, M.E.; Kucukbayrak, S. Effects of electrospinning parameters on gelatin/poly(epsilon-caprolactone) nanofiber diameter. *Chem. Eng. Technol.* **2015**, *38*, 844–850. [CrossRef]
34. Mo, G.-Z.; Wu, Y.-C.; Hao, Z.-F.; Luo, Q.-F.; Liang, X.-Y.; Guan, L.-T.; Wang, Z.-Y. Synthesis and characterization of a novel drug-loaded polymer, poly(lactic acid-co-aminomethyl benzimidazole). *Des. Monomers Polym.* **2015**, *18*, 536–544. [CrossRef]
35. Wei, K.; Kim, H.K.; Kimura, N.; Suzuki, H.; Satou, H.; Lee, K.H.; Park, Y.H.; Kim, I.S. Effects of organic solvent and solution temperature on electrospun polyvinylidene fluoride nanofibers. *J. Nanosci. Nanotechnol.* **2013**, *13*, 2708–2713. [CrossRef] [PubMed]
36. Kanani, A.G.; Bahrami, S.H. Effect of changing solvents on poly(epsilon-caprolactone) nanofibrous webs morphology. *J. Nanomater.* **2011**, *2011*, 724153:1–724153:10.
37. Yu, Y.S.; White, J.L. Comparison of structure development in quiescent crystallization, die extrusion and melt spinning of isotactic polypropylene and its compounds containing fillers and nucleating agents. *Polym. Eng. Sci.* **2001**, *41*, 1292–1298. [CrossRef]
38. Wang, C.; Jheng, J.H.; Chiu, F.C. Electrospun nylon-4,6 nanofibers: Solution rheology and brill transition. *Colloid Polym. Sci.* **2013**, *291*, 2337–2344. [CrossRef]